Global Biogeochemical Cycles®

RESEARCH ARTICLE
10.1029/2024GB008218

New Deoxygenation Threshold for N_2 and N_2O Production in Coastal Waters and Sediments

Ludovic Pascal[1], **Félix Cloutier-Artiwat**[1], **Arturo Zanon**[1], **Douglas W. R. Wallace**[2], and **Gwénaëlle Chaillou**[1]

[1]Québec Océan, Institut des Sciences de la Mer de Rimouski (ISMER), Université du Québec à Rimouski, Rimouski, QC, Canada, [2]Department of Oceanography, Dalhousie University, Halifax, NS, Canada

Key Points:

- Fixed-N is possibly removed in suboxic (<5 μM) microzones on suspended organic matter at bulk O_2 of 32–59 μM in the St. Lawrence Estuary
- Benthic and possibly water column fixed-N removal processes drive a strong NO_3^- deficiency in bottom waters of the St. Lawrence Estuary
- Significant net production of N_2O was observed in bottom waters of the St. Lawrence Estuary when ambient O_2 fell below 59 μM

Supporting Information:

Supporting Information may be found in the online version of this article.

Correspondence to:

L. Pascal,
ludovic_pascal@uqar.ca

Citation:

Pascal, L., Cloutier-Artiwat, F., Zanon, A., Wallace, D. W. R., & Chaillou, G. (2025). New deoxygenation threshold for N_2 and N_2O production in coastal waters and sediments. *Global Biogeochemical Cycles*, *39*, e2024GB008218. https://doi.org/10.1029/2024GB008218

Received 8 MAY 2024
Accepted 22 JUL 2025

Author Contributions:

Conceptualization: Ludovic Pascal, Gwénaëlle Chaillou
Data curation: Ludovic Pascal, Gwénaëlle Chaillou
Formal analysis: Ludovic Pascal, Félix Cloutier-Artiwat, Arturo Zanon, Gwénaëlle Chaillou
Funding acquisition: Ludovic Pascal, Douglas W. R. Wallace, Gwénaëlle Chaillou
Investigation: Ludovic Pascal, Gwénaëlle Chaillou
Methodology: Ludovic Pascal, Gwénaëlle Chaillou
Project administration: Ludovic Pascal, Douglas W. R. Wallace, Gwénaëlle Chaillou

Abstract Bioavailable nitrogen governs ocean productivity and carbon fixation by regulating phytoplankton growth and community composition. Nitrogen input primarily results from N_2 fixation, while denitrification and anammox remove bioavailable nitrogen in oxygen-depleted conditions. Traditionally considered limited to highly suboxic (i.e., <5 μM) waters, recent studies suggest that fixed-nitrogen removal processes may extend beyond, elevating global nitrogen loss estimates. This study directly quantifies fixed-nitrogen loss across oxygen gradients (from 140 to 32 μM) along the Estuary and Gulf of St. Lawrence using N cycle tracers (N_2/Ar, N^*, and N_2O). Notably, we observe significant N_2 production when ambient O_2 concentrations fall below a threshold value of 58.9 ± 1.1 μM, including potential water column fixed-nitrogen removal processes above suboxia. We hypothesis that ambient deoxygenation eases the formation of suboxic microareas in suspended organic matter. Benthic N_2 production remains unaffected under intensifying water column deoxygenation from 50 down to 32 μM, but the contribution of NO_3^- produced through nitrification in the sediment to denitrification diminishes as deoxygenation intensifies. Combined, water column and benthic fixed-nitrogen removal processes drive N^* anomalies and strong NO_3^- deficiency in bottom waters. Additionally, the observed O_2 threshold also triggers N_2O production. Overall, our study highlights the profound impact of coastal ocean deoxygenation on nitrogen cycling, suggesting unexpected shifts even at ambient oxygen concentrations traditionally considered well above suboxic conditions.

Plain Language Summary This study explores processes that influence the availability of nitrogen, a limiting key nutrient for algal production and the biological carbon pump in the ocean. It focusses on nitrogen loss mechanisms which remove bioavailable nitrogen under barely detectable oxygen levels. Contrary to previous assumptions limiting these mechanisms to very low oxygen levels, this research suggests, in natural conditions, that nitrogen loss mechanisms can potentially occur in environments with higher ambient oxygen levels, challenging our understanding of nitrogen cycling. This study uses multiple nitrogen cycle tracers coupled with sediment core incubations to quantify nitrogen loss in the Estuary and Gulf of St. Lawrence. The findings include substantial bioavailable nitrogen loss and nitrous oxide production in the hypoxic water column as well as strong nitrate deficiency. This nitrogen loss can have broad implications and impact the growth and productivity of algae at the ocean surface. These insights will help to better predict the role of the ocean in the context of climate change.

1. Introduction

Bioavailable (or fixed) forms of nitrogen (N), including nitrite (NO_2^-), nitrate (NO_3^-), ammonium (NH_4^+) and organic nitrogen, exert a major control on ocean and estuary productivity, and thereby carbon fixation, by governing phytoplankton growth rates and community composition in surface waters (Bowen et al., 2020; Moore et al., 2013). Typically, N inputs in the ocean come from several sources, including N_2 fixation by diazotrophic organisms (e.g., cyanobacteria), rivers, groundwaters and particles transported by the wind. This fixed N is generally conserved within the ocean, in its various organic and inorganic forms. Under oxygen-depleted conditions (i.e., suboxia or O_2 < 5 μM), anaerobic microorganisms use NO_3^- and/or NO_2^- as electron acceptors, converting bioavailable nitrogen to gaseous N_2, effectively removing it from ocean inventories (Devol, 2015). However, uncertainties persist whether or not the marine nitrogen budget is currently balanced (Codispoti, 2007; DeVries et al., 2012) leading to significant ambiguity regarding how it may respond to climate change, both globally and regionally (Hutchins & Capone, 2022). This ambiguity is largely due to the incomplete understanding of the nitrogen cycle and its environmental controls. This cycle involves numerous microbial

Resources: Douglas W. R. Wallace, Gwénaëlle Chaillou
Software: Ludovic Pascal
Supervision: Ludovic Pascal, Douglas W. R. Wallace, Gwénaëlle Chaillou
Validation: Ludovic Pascal, Douglas W. R. Wallace, Gwénaëlle Chaillou
Visualization: Ludovic Pascal
Writing – original draft: Ludovic Pascal
Writing – review & editing: Ludovic Pascal, Félix Cloutier-Artiwat, Arturo Zanon, Douglas W. R. Wallace, Gwénaëlle Chaillou

transformations between organic and inorganic nitrogen solutes occurring under various redox conditions, which can be impacted by physical effects on microbial populations (e.g., Haas et al., 2019).

In marine systems, denitrification and anaerobic ammonia oxidation (anammox) are the main pathways converting fixed N to N_2. Anammox is a chemolithoautotrophic pathway that utilizes the energy generated during the conversion of NH_4^+ to N_2 using NO_2^- to assimilate inorganic carbon. Denitrification, operating as a heterotrophic pathway, sequentially reduces NO_3^- to NO_2^-, NO, and N_2O gases, ultimately yielding N_2. This pathway is mediated by facultative anaerobic microorganisms using NO_3^- as an alternative electron acceptor when O_2 is scarce. Beyond its function as a nitrogen sink, heterotrophic denitrification is recognized as one of the principal mechanisms driving remineralization in sedimentary environments (Middelburg & Levin, 2009). Additionally, dissimilatory nitrate reduction to ammonium (DNRA) is another microbial transformation wherein NO_3^- is reduced to NH_4^+. This alternative pathway retains fixed-nitrogen in oxygen-depleted environments although the newly formed NH_4^+ can subsequently fuel anammox (Hardison et al., 2015). Because aerobic respiration outcompetes nitrogen-reducing processes under oxygenated conditions, a large portion of the ocean bioavailable N loss takes place in sedimentary environments (Middelburg et al., 1996), and in oxygen minimum zones (OMZs; Lam & Kuypers, 2011). Recent modeling and laboratory studies have shown that denitrification and anammox (hereafter referred to as "fixed-N removal processes") can take place in suboxic microenvironments even when ambient oxygen concentrations are well above the suboxic threshold (Bianchi et al., 2018; Ciccarese et al., 2023; Smriga et al., 2021; Stief et al., 2016, 2017). However, investigations are required to assess the significance of this particular process in the natural environment as well as its environmental controls. In the broader context of global ocean deoxygenation, characterized by the expansion of OMZs and declining oxygen levels in coastal and open-ocean waters (Breitburg et al., 2018), the potential widespread occurrence of fixed-N removal processes beyond traditionally-defined suboxic water columns assumes critical significance. This goes beyond the anticipated expansion of OMZs and enhanced benthic fixed-N removal process rates associated with deoxygenation. This suggests that such processes may occur under a broader range of oxygen conditions than previously assumed. This may have implications for how current estimates of global N loss are interpreted and constrained. This challenge current assumptions about the environmental boundaries and controls on fixed-N removal processes in the ocean (Bianchi et al., 2018). The tight interplay between nitrogen availability, and primary production (Moore et al., 2013) adds another layer to this complexity. The potential alteration of nitrogen cycling, particularly fixed-N removal processes, could reshape assumptions regarding carbon exchanges between the atmosphere and the ocean. This, in turn, may have far-reaching implications for ocean productivity and its role in the context of climate change. In light of these considerations, the urgency for field studies to directly quantify fixed-N removal processes across oxygen gradients becomes readily apparent. Such investigations are essential for unraveling the complex interplay between oxygen availability and nitrogen cycling in marine ecosystems, ultimately enhancing our understanding of the broader implications of deoxygenation on global nitrogen budgets and climate change.

This study aims to evaluate the potential for water column and benthic fixed-N removal processes to occur under declining oxygen concentrations in the natural environment. We used three key tracers of marine nitrogen cycling (N_2/Ar, N_2O, N^*) in combination with sediment core incubation and micro-profiling. N_2/Ar, a denitrification tracer, uses the analogous behavior of N_2 and Ar to most physical processes and thus primarily captures the biological production (or fixation) of N_2. N^* quantifies the excess or deficiency of fixed nitrogen relative to phosphate, providing insights into the alteration of this stochiometric ratio which may influence community structure of primary producers (Hecky & Kilham, 1988). N_2O, a potent greenhouse gas (GHG), is an indicator of incomplete denitrification, particularly due to the inhibition of nitrous oxide reductase in the presence of O_2 (Bonin et al., 1989). However, low O_2 concentrations can also enhance N_2O production during nitrification (Punshon & Moore, 2004; Zhou et al., 2023). Thus, changes in N_2O concentration serve as an indicator of altered nitrogen cycling dynamics.

Our measurements were carried out in the deep waters along the Estuary and Gulf of St. Lawrence (EGSL). In the last century, EGSL has experienced a substantial decline in its bottom-water oxygen concentrations at the most oxygen depleted zone, plummeting from around 125 μM in the 1930s to an average of 65 μM between 1984 and 2003, further decreasing to around 35 μM by 2021 (Jutras, Mucci, et al., 2023). Aside from biogeochemical transformations playing a crucial role in oxygen depletion until the late 1990s, a large-scale forcing of the Labrador Current retroflexion has emerged as the dominant factor since 2008 (Jutras, Dufour, et al., 2020, 2023; Jutras, Mucci, et al., 2023). Presently, the severity of hypoxia (i.e., O_2 concentration <62.5 μM) varies spatially,

with a landward oxygen concentration gradient ranging from relatively normoxic bottom waters in the Gulf (~140 μM) to severely hypoxic conditions (~35 μM) at the head of the Lower St. Lawrence Estuary. Consequently, the EGSL stands as a distinctive natural laboratory, offering a unique opportunity to investigate the impact of in situ deoxygenation on nitrogen cycling. Here we postulate that the deoxygenation of bottom waters in the EGSL limits oxygen availability at the sediment surface, leading to a progressive increase in sedimentary N_2 production. Simultaneously, we anticipate a reduction in sedimentary nitrification, causing a decline in the NO_3^- stock both in porewater and the overlying water column, which would consequently alter the stochiometric ratio between N and P. Additionally, we propose that water column fixed-N removal processes are confined to the most oxygen depleted zone, contributing minimally to the overall N_2 production.

2. Methods and Data

2.1. Study Site

The present study was carried out in the St. Lawrence Estuarine System (Canada) and, more precisely, in the Laurentian Channel (LC; Figure 1). This deep (250–500 m) and long (1,240 km) glacially-carved submarine valley stretches along the Estuary and Gulf of St. Lawrence from the continental shelf break to the mouth of the Saguenay Fjord near Tadoussac (Figure 1b), where the bathymetry shoals abruptly (Koutitonsky & Bugden, 1991). The water column in this area is strongly stratified (Figure S2 in Supporting Information S1), consisting of three distinct layers. A relatively fresh, summer-warm surface water (0–50 m) flowing seaward overlying a cold intermediate layer formed by winter cooling of surface water to near-freezing temperature in the Gulf (50–150 m deep), which flows landward together with a warmer and saltier bottom water layer (>150 m; Figure S2 in Supporting Information S1). The bottom waters originate as a mixture of cold, oxygen-rich waters from the Labrador Current Water (LCW) and relatively oxygen-depleted, warmer waters from the North Atlantic Central Water (NACW), which is formed at the edge of the continental shelf in the northwest Atlantic Ocean. This mixture travels along the LC. Upon reaching the head of the LC, the local bathymetry and tidal forces drive the upwelling of these bottom waters. The upwelled waters then mix with less dense surface waters, and this process, combined with strong water column stratification, fuels the estuarine circulation of the St. Lawrence, pulling more LCW and NACW from the shelf edge into the system. The travel time of bottom waters from the edge of the continental shelf to the head of the LC is about 4.7 years based on results of a recent tracer release experiment (Stevens et al., 2024) in relative good agreement with previous models (Bugden, 1991; Gilbert, 2004; Rousseau et al., 2025). During this journey, the deep waters are isolated from the atmosphere by a permanent pycnocline (Petrie et al., 1996). As a result, oxygen concentrations decline landward as a result of respiration and organic matter mineralization (Gilbert et al., 2005).

2.2. Sampling Procedure

Samples were collected on-board the R/V *Coriolis II* during multiple scientific cruises during summer 2021, 2022, and 2023 (Figure S1 in Supporting Information S1). A Conductivity-Temperature-Depth sensor (CTD, Seabird® SBE 911plus, Bellevue, Washington, USA) and oxygen probe (Seabird® SBE-43) were mounted on a 12 × 12 L Niskin-bottles rosette to record depth profiles of temperature, salinity, pressure, and oxygen concentration of the water column at each station (Figure 1b). Although the oxygen probe had been calibrated by the manufacturer within the year, discrete water samples were collected through the water column to calibrate the oxygen sensor using Winkler titrations, following Grasshoff et al. (1999) procedure as detailed in Jutras, Dufour, et al. (2023) and Jutras, Mucci, et al. (2023). Niskin bottles were closed within 10 m above the seafloor at each station.

Water samples were collected in duplicated 12 mL Exetainers® (Labco Limited, Ceredigion, UK) and poisoned by introducing 200 μL of a 7 M $ZnCl_2$ solution and stored at 4°C prior to dissolved gas (i.e., N_2 and Ar) measurements. Water samples for N_2O analysis were collected in 20 mL clear glass round bottom vials and poisoned using 50 μL of mercury chloride ($HgCl_2$). Vials were immediately crimped sealed, avoiding air bubbles. In addition, water samples were collected in 15 mL vials and stored at −20°C for further nutrients (i.e., NO_3^-, NO_2^-, PO_4^{3-}) analyses. In 2021, additional bottom water was collected into air-tight plastic bags and stored in the dark at bottom seawater temperature (~6°C) for later use to replace water withdrawn during sediment core incubations.

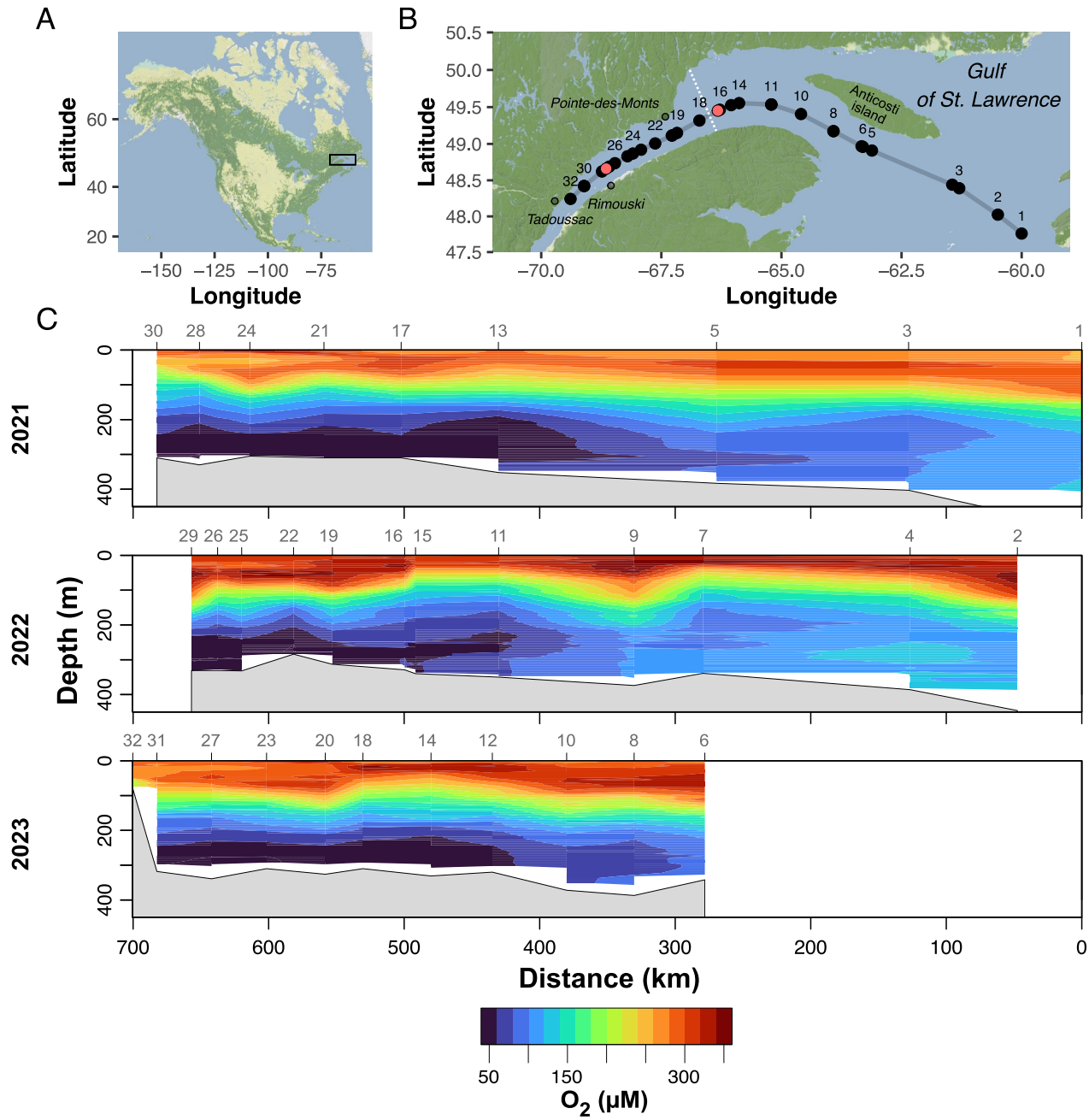

Figure 1. Study site. (a) Location of the Estuary and Gulf of St. Lawrence (black rectangle) and (b) sampled stations (projection Mercator). Black circles indicate stations where bottom water was collected and red circles indicate stations where sediment core for incubation was collected. The dotted white line represents the location of the O_2 concentration breakpoint identified for the 2021–2023 period. The portion of the transect west of the breakpoint corresponds to the segment below the $[O_2]$ threshold, while the portion east corresponds to the segment above the $[O_2]$ threshold. (c) Water column oxygen concentration along the Laurentian Channel in 2021, 2022, and 2023. Map tiles by Stamen Design® and map data by OpenStreetMap®.

In 2021, sediment samples were collected at stations 17 and 28 using one large (50 × 50 × 60 cm) and one small (30 × 40 × 50 cm) Ocean Instrument® Mark II box corers. These two stations were selected because they represented the extremes of oxygen concentrations within the hypoxic area. At each station, seven sediment cores were sub-sampled within the large box corer using transparent acrylic tubing (10 cm inner diameter, 40 cm long). The level of sediment compression resulting from the tubing insertion was always <0.5 cm. The sediment surface within the large sediment cores was immediately capped with Styrofoam® and the tubing was hermetically sealed with rubber lids to limit contact with the atmosphere. Within 15 min, sediment cores were collected, brought back

to the on-board thermo-regulated (6°C) laboratory in the dark and gently filled (*ca.* 1 L per core) with the previously collected bottom water. Six sediment cores were kept intact to assess total benthic fluxes at the sediment-water interface. The remaining sediment core was connected to a N_2 bubbling system controlled by an O_2 monitoring/regulator device (OXY-REG, Loligo Systems®, Viborg, Denmark) to maintain in situ O_2 conditions during O_2 micro-profiling at the SWI (see below).

At each station, the whole small box corer was transferred to a glove box continuously flushed with N_2 to limit sediment oxidation. The whole surface area (30 × 40 cm) except for the edge of the core in contact with the box corer was used for porewater extraction. The core was sub-sampled at 0.5 cm intervals over the top two cm, at 1 cm intervals down to 5 cm, at 2 cm intervals down to 15 cm and then at 5 cm intervals down to the end of the sediment core. Sub-samples were transferred to a Reeburgh-type squeezer to extract pore water (Reeburgh, 1967). Briefly, a pressure of 250–400 kPa N_2 was exerted on a gas-tight membrane squeezing the sediment against a 0.45 µm polycarbonate filter. The pore water was directly collected into a pre-washed 50 mL syringe, which was hermetically attached at the output of the squeezer, transferred into a 5 mL cryovial, and stored at −80°C for later porewater nutrient analysis.

2.3. Intact Core Incubation Experiments

First, an initial water sample was collected in the overlying water of four cores to determine the ambient NO_3^- concentration prior to the addition of the isotope tracer. A certain volume of a 20 mM $^{15}N - NO_3^-$ solution (99% atom $^{15}N - NaNO_3^-$, Sigma-Aldrich®) was added in the overlying water of each of these four cores to achieve a nominal concentration corresponding to 50% and 100% of the ambient concentration in two sets of intact sediment core incubations ($n = 2$ in each set). Given the thin oxic sediment layer (OPD <2 mm), a pre-incubation period of 1h was performed to ensure adequate diffusion of $^{15}N - NO_3^-$ to the sediment nitrate reduction zone (Nielsen, 1992). During this period, a He bubbling system controlled by an O_2 monitoring/regulator maintained in situ O_2 conditions until the start of the incubation. After the pre-incubation period, a water sample was collected to determine the exact concentration of $^{15}N - NO_3^-$ and the initial $^{29}N_2$ and $^{30}N_2$ concentrations. The incubation was then immediately initiated by fitting the six sediment cores (four amended with the addition of $^{15}N - NO_3^-$ and two that had not been amended) with PVC lids equipped with magnetic stirrers. The O_2 concentration in overlying incubated water was measured continuously using calibrated optodes (Oxygen sensor Spot SP, PreSens®) connected to an OXY-10 SMA (PreSens®) through optical fibers. Incubations were performed in the dark at the bottom water temperature. The incubation duration was adjusted so that O_2 saturation in the overlying water never dropped below 80% of its initial value (typically 12 hr). During the incubations, 5 discrete water samples were collected at 3 hr intervals, filtered (0.2 µm) and stored at −80°C for nutrient analyses. In amended sediment cores, additional water samples were collected in 12 mL Exetainers®, poisoned with 200 µL of 7 M $ZnCl_2$ and stored at slightly sub-ambient temperature (4°C) for further $^{29}N_2$ and $^{30}N_2$ analyses. Water removed during sampling (<6% of the overlying volume over the incubation) was automatically replaced with previously collected bottom water maintained at in situ O_2 level. The dilution effect of discrete sampling was corrected in our flux calculations. At the end of the incubations, the remaining water was mixed with the top 5 cm of the sediment column. From the slurry, 12 mL of sample was transferred to an Exetainer to which 200 µL of 7 M $ZnCl_2$ were added for further $^{15}N - NH_4^+$ analysis. The slope (in mmol m^{-3} hr^{-1}) from the linear regression of the changes in O_2, nutrients and $^{29,30}N_2$ concentrations over incubation duration was used to compute benthic fluxes as follows:

$$J_{\text{benthic}} = \text{slope} \times \frac{V}{A}$$

where J_{benthic} is the benthic flux across the sediment-water interface (mmol m^{-2} d^{-1}), V is the volume of overlying water in the experimental enclosure (m^3), and A is the surface of the sediment-water interface (m^2). Since no difference in O_2 and nutrient fluxes between amended and non-amended sediment cores was detected, the fluxes from all 6 replicates were used.

Since no production of $^{15}N - NH_4^+$ was detected over the incubation periods, DNRA was considered to be negligible. The validity of the original isotope pairing technique (IPT; Nielsen, 1992) was tested by checking the independence of the estimated $^{28}N_2$ production and the amount of added $^{15}N - NO_3^-$ (Nielsen, 1992; Risgaard-Petersen et al., 2003). Potential denitrification rates were calculated following Nielsen (1992):

$$D_{15} = p29 + 2 \times p30$$

where D_{15} is the denitrification rate of the $^{15}N - NO_3^-$ and $p29$ and $p30$ are the production of $^{29}N_2$ and $^{30}N_2$, respectively.

$$D_{14} = D_{15} \times \frac{p29}{2 \times p30}$$

where D_{14} is the denitrification rate of $^{14}N - NO_3^-$. From D_{14} and D_{15}, the denitrification of nitrate diffusing from the overlying water to the nitrate reduction zone (D_w) and the denitrification of nitrate produced within the sediment through nitrification (D_n) were calculated as follows:

$$D_w = \frac{^{14}NO_3^-}{^{15}NO_3^-} \times D_{15}$$

$$D_n = D_{14} - D_w$$

where $^{14}NO_3^-$ is the ambient nitrate concentration and $^{15}NO_3^-$ is the concentration of labeled nitrate added to the overlying water. Total denitrification (D_{tot}) was calculated as the sum of D_w and D_n

$$D_{tot} = D_w + D_n$$

2.4. Sediment O_2 Micro Profiling

Oxygen concentration within the sediment was measured using Clark-type micro-microelectrodes. At least 5 depth profiles of O_2 concentration were randomly performed in one large sediment core. This sampling design was chosen because it has been shown that biogeochemical heterogeneity of the sediment is often associated with micro-environments (Stockdale et al., 2009). OX-100 micro-electrodes (Unisense®) were inserted using a motor-driven micro-manipulator (MU1, Pyroscience®) set up with steps of 100 µm. Linear calibration was achieved between the oxygen concentration of air-bubbled bottom water (100%) and the anoxic area of the sediment (0%). During profiling, the overlying water was connected to the N_2 bubbling system. O_2 micro-profiling was typically completed within 30–60 min of core recovery. O_2 diffusive fluxes (J_{diff} in mmol m^{-2} hr^{-1}) were computed using probeflux software (Deflandre & Duchêne, 2010) based on Fick's first law as described in the following equation:

$$J_{diff} = \varnothing \times \frac{D_0}{1 + 3(1 - \varnothing)} \times \frac{\delta C}{\delta z}$$

where ϕ is the sediment porosity, D_0 is the diffusion coefficient (m^2 hr^{-1}) of O_2 in water and $\frac{\delta C}{\delta z}$ is the concentration gradient (mmol m^{-3} m^{-1}) directly below the sediment water interface. J_{diff} values for nutrients were calculated similarly using the concentration gradient between the bottom waters and the first sample below the sediment water interface (typically at 0.5 cm).

2.5. Sample Analyses

N_2/Ar, $^{29}N_2$, and $^{30}N_2$ measurements were completed within 2 months of collection, with most samples analyzed within 1 month, using a membrane inlet mass spectrometer (MIMS, Bay Instruments®, Easton, Maryland, USA) (Kana et al., 1994). The protocol followed (Kana et al., 2006). Briefly, the water samples were pumped through stainless steel tubing, which was connected to a gas-permeable membrane tube within the vacuum inlet, and both immersed in a thermos-regulated water bath (6°C) to assure a constant sampled water temperature at the membrane level. The gas stream goes through a U-shape tube immersed in liquid nitrogen (cryotrap) to remove H_2O vapor. Then the gas stream enters a copper reduction column heated to 600°C to remove O_2 and thus avoid any potential effects of O_2 interference on the N_2/Ar ratio (Eyre et al., 2002). Eventual CO_2 and CO produced in the copper reduction column were removed using another cryotrap prior to entering the Pfeiffer Vacuum quadrupole mass spectrometer. Calibration was achieved by sampling a 1 L spherical flask containing *ca.* 500 mL

of freshly prepared, filtered in situ seawater immersed in the same thermoregulated bath (6°C) containing the membrane inlet. The flask opening was fitted with a damped sponge to ensure saturated air humidity, and the water was constantly stirred with a stirrer paddle without generating bubbles. N_2/Ar ratios were determined by analyzing masses 28 ($^{28}N_2$) and 40 (^{40}Ar). Calibration factors for the standard sample were computed based on solubility equations (Hamme & Emerson, 2004). To quantify the production of $^{15}N - NH_4^+$, the water samples were first gently bubbled with He during 5 min to remove all $^{15}N - N_2$ produced during the incubation. The water samples were then treated with alkaline hypobromite to oxidize NH_4^+ to N_2 prior to analysis using MIMS as described in Yin et al. (2014). Before analysis, vials were checked for bubbles as indicators of seal failure and data from vials showing seal failure were excluded.

N_2O measurements were performed using headspace gas chromatography (GC) and electron capture detection with an Agilent 7890B Series Gas Chromatograph and Agilent 7597A headspace sampler. Exactly 10 mL of seawater was displaced from the vials with helium gas to introduce a headspace and samples were shaken on a bench top shaker for 10 min to allow for initial equilibration. Following this, samples were placed in the headspace autosampler where samples were maintained at 40°C for 15 min and then pressurized at 22 psi using N_2 for 10 min. The pressurized headspace gas was released into a 1 mL gas sample loop and transferred to the GC, which was equipped with a poraPLOT Q-HT 25 m × 0.32 mm × 10 µm column from Agilent Technologies. The GC was calibrated using injections of two high-pressure gas standards with known mole fractions of nitrous oxide in nitrogen gas (0.5 and 1 ppm). The mole fractions of the two gas standards were determined by Praxair. Calculation considered the partitioning of N_2O between the water sample and headspace at the pressure and temperature of equilibration. The precision of the water measurements was estimated to be ±0.9 nM as calculated from the standard deviations based on the triplicate analyses.

NO_3^- (quantification limit 0.6 µM), NO_2 (quantification limit 0.01 µM), NH_4^+ (quantification limit 0.1 µM) and PO_4^{3-} (quantification limit 0.1 µM) samples were analyzed using an autoanalyzer AA500 (Seal analytical®, Norderstedt, Germany), following (Aminot et al., 2009).

2.6. Conceptual Model

2.6.1. Model Definition

In this study, we hypothesized that the bottom water of the EGSL acts as a closed system completely isolated from the surface layers over the sampled transect. This is supported by our temperature, salinity, density (Figure S4 in Supporting Information S1) and Argon (Figure S5 in Supporting Information S1) data. This closed system assumption implies that changes in N_2, O_2, and N_2O concentrations are directly linked to in situ biological processes and exchanges with the underlying sediment rather than physical changes. We also considered that the age of the bottom water is proportional to the distance along the transect. A vertical extension of the water layer in our conceptual model was determined by visually assessing gradients in ΔN_2/Ar, O_2, temperature, and salinity profiles from water column measurements at station 28 (Figure S6 in Supporting Information S1). A distinct gradient was observed at approximately 200 m depth, indicating a potential mixing zone and transition between water masses. The vertical extent of the water layer was quantified as 118.32 m, calculated by averaging the distance between the observed gradient depth (i.e., 200 m) and the bottom of the water column across multiple sites in the hypoxic area. Under those assumptions, changes in gas composition in the water column can be expressed as

$$J_{\text{net}} = \frac{J_{\text{benthic}}}{z} + J_w$$

where J_{benthic} is the areal benthic flux as described above, z is the vertical extent of the conceptual model, J_w (in mmol m^{-3} hr^{-1}) is the volumetric flux in the water column due to biological processes, and J_{net} (in mmol m^{-3} hr^{-1}) is the volumetric flux in the system also expressed as

$$J_{\text{net}} = \frac{\delta C}{\delta x} \times F_r$$

where $\frac{\delta C}{\delta x}$ is the slope of the relationship between the dissolved gas (i.e., O_2 or N_2) and the cumulative distance along the transect, and F_r is the flow rate of the water mass (0.018 km hr^{-1}; Stevens et al., 2024), allowing conversion of the spatial gradient to a volumetric flux.

2.6.2. Model Uncertainties

The St. Lawrence Estuary's dimensions, bathymetry (circulation patterns), and permanent oxygen concentration gradient make it a unique natural laboratory for studying the biogeochemical impact of ocean deoxygenation (Pascal et al., 2023). Previous studies using conceptual models similar to ours, although more complex, have yielded results consistent with observational data (Jutras, Dufour, et al., 2020; Jutras, Mucci, et al., 2020, 2023). Our model's assumptions are supported by our data (see previous section), as well as in situ turbulence measurements, numerical models and the monitoring of inert chemical tracers (Bluteau et al., 2021; Bourgault et al., 2012; Cyr et al., 2011, 2015; Stevens et al., 2024). However, we acknowledge certain limitations and uncertainties:

First, at the head of the LC near Tadoussac, bathymetric features and tidal currents drive strong upwelling of bottom water, resulting in mixing between dense bottom waters and less dense surface waters (Saucier et al., 2009). Although upwelling is the dominant current, the ebb tide can also induce episodic downwelling, returning part of the mixed waters toward the bottom of the LC, which may influence the biogeochemical signals measured in this study. To assess this potential influence, the water mass endmembers were first identified using a temperature–salinity diagram (Figure S1 in Supporting Information S1). Mixing proportions were then quantified, and the corresponding contribution to the observed biogeochemical signals was estimated (see Supporting Information S1). The analysis indicates that although mixing can be detected, its impact is negligible. For example, it accounts for ∼9% of the observed increase in N_2 concentrations (see Supporting Information S1).

Second, our model assumes a unidirectional net average bottom water flow based not only on previous biogeochemical and numerical models (Bugden, 1991; Gilbert, 2004; Jutras, Mucci, et al., 2020) but also on recent tracer release experiments (Stevens et al., 2024). The estimate based on the tracer release experiment encompasses turbulent mixing, seasonal changes, and small-scale transport processes over a 12-month period. However, tidal forcing introduces oscillatory movements, leading to variability in actual water transit times. This variability could affect the precise spatial distribution of biogeochemical signals, although it is unlikely to alter the overall observed trends. Local currents, such as the presence of several gyres, may cause deviations from this simplified assumption. The strongest of these, the Anticosti Gyre, is located in the western Gulf. Numerical simulations suggest that while the Anticosti Gyre's influence can extend into the bottom waters (>100 m), particularly during winter, the current strength decreases significantly with depth (Galbraith et al., 2024). A recent modeling study shows that the Anticosti Gyre indeed influences the bottom water flow (Rousseau et al., 2025), but it does not result in an extended transit time of deep waters in the LC compared to the estimate based on tracer observation by Stevens et al. (2024). Downwelling at the head of the Laurentian Channel introduces additional complexity by increasing bottom water residence time and enhancing mixing with the overlying intermediate cold layer. In our conceptual model, an increase in residence time can be assimilated to a decrease in the net average bottom water flow. This decrease in flow would lower J_{net} and the contribution of J_w to J_{net}, since $J_{benthic}$ is based on direct measurements and thus independent of the net average bottom water flow. To assess the model's sensitivity to deviations from unidirectional flow, we reduced the net average bottom water flow by a factor of three and increased the theoretical mixing by a factor of three. For N_2, this led to a reduction in the contribution of J_w to J_{net} by up to 16%, but did not significantly alter our overall interpretation of the data.

Overall, the available data and understanding of flow dynamics within the LC suggest that our conceptual model is robust, with any deviations from the assumptions being unlikely to significantly affect the observed trends or conclusions.

2.7. Data Analyses

2.7.1. Computation of Nitrogen Cycling Proxies

Three tracers of nitrogen cycling were used during this study: N_2/Ar, N_2O, and N* focusing on denitrification products (i.e., N_2 and N_2O) and reactants (i.e., NO_3^-), respectively. The N_2/Ar ratio was first expressed as the

N_2/Ar supersaturation (Hamme & Emerson, 2013), a normalized ratio calculated as the anomaly from the expected ratio at equilibrium:

$$\Delta N_2/Ar = \frac{N_2/Ar_{meas}}{N_2/Ar_{equil}} - 1$$

where N_2/Ar_{meas} is the measured N_2/Ar ratio, N_2/Ar_{equil} is the N_2/Ar ratio at equilibrium with the atmosphere at the temperature and salinity of the water mass (Hamme & Emerson, 2004). In this study, the supersaturation ratio is presented in percent (the ratio is $\times 100$). N_2 and N_2O concentrations along the Laurentian Channel were expressed as δ (δN_2 and δN_2O) corresponding to the difference in corresponding gas concentration relative to the concentration at the reference point (Station 1) at the easternmost point of the transect. Given our model assumption, δN_2 and δN_2O correspond to N_2 and N_2O excess along the Laurentian Channel

N* was computed following Gruber and Sarmiento (1997):

$$N^* = \left[NO_3^-\right] - 16 \times \left[PO_4^{3-}\right] + 2.9$$

where 2.9 corresponds to a constant allowing the N^* of the global ocean to equal 0. NO_2^- and NH_4^+ were not included in the equation because their concentrations were often below the quantification limit of our analyses.

2.7.2. Statistical Analyses

Data values are given as mean ±SE. CTD data (localization, depth, oxygen, temperature and salinity) were processed and visualized using the *oce* R-package (Kelley & Richards, 2022). The station positions were adjusted so that all stations are located along a common transect (average transect), using a general additive model (*gam* function from *mgcv* R-package; Wood, 2017) applied to longitude and latitude data (actual locations of sampled stations are presented in Figure S1 in Supporting Information S1). This model estimated the corrected latitude for each station, ensuring that the corrected location of each station coincided with the average transect. On average, this adjustment resulted in a displacement of 4.5 ± 3.9 km. From the corrected location, the cumulative distance along the transect was computed using *geodDist* function from *oce* R-package. Station 1 was set as the reference point and corresponded to km 0 of this 743.54 km long transect. Given the similarity of data from 2021, 2022, and 2023, all results were combined for a streamlined analysis. Figure 1 presents water column O_2 concentrations from the 3 years separately to emphasize their comparable nature. The supersaturation ratio was used to accurately assess the position of a breakpoint in the relationship between ΔN_2/Ar and the cumulative distance along the transect. The existence of a breakpoint in the relationship between cumulative distance along the transect and ΔN_2/Ar was tested using a Davies test (Davies, 2002) and a segmented linear model was fitted to the data to accurately locate the breakpoint using the *segmented* function from *segmented* R-package (Muggeo, 2017). For O_2, a single linear model was then applied to the data using *lm* function from *stat* R-package (RCore Team) due to its linear decrease along the transect. For all other gases (N_2, N_2O) and nutrient variables, linear models were then similarly fit to the data before and after the breakpoint. The normality of the distribution and the homoscedasticity of the residuals as well as the presence of outliers were tested for each model. No deviation from the model assumption was observed.

Linear models were fitted to test the effect of *Station* (fixed factor; two levels) on benthic fluxes ($J_{benthic}$) and denitrification rates (D_{tot}). The normality and homoscedasticity of the residuals and the presence of outliers were tested for each model. Then, the degrees of freedom, sum of squares *F*-statistic and associated *p*-value of each term were computed using the *anova* function from *stats* R-package.

3. Results

3.1. Bottom Water Dissolved Gas Concentrations

Gas concentration in the bottom waters along the Laurentian Channel (LC) increased non-linearly, with a breakpoint in the relationship located 516.2 ± 23.9 km along the sampled transect (Figure 2). Hereafter, the transect is divided into two sections by the breakpoint, with the segment above the [O_2] threshold to the east (0–516.2 km) and the segment below the [O_2] threshold to the west (516.2–750.9 km). The O_2 concentration

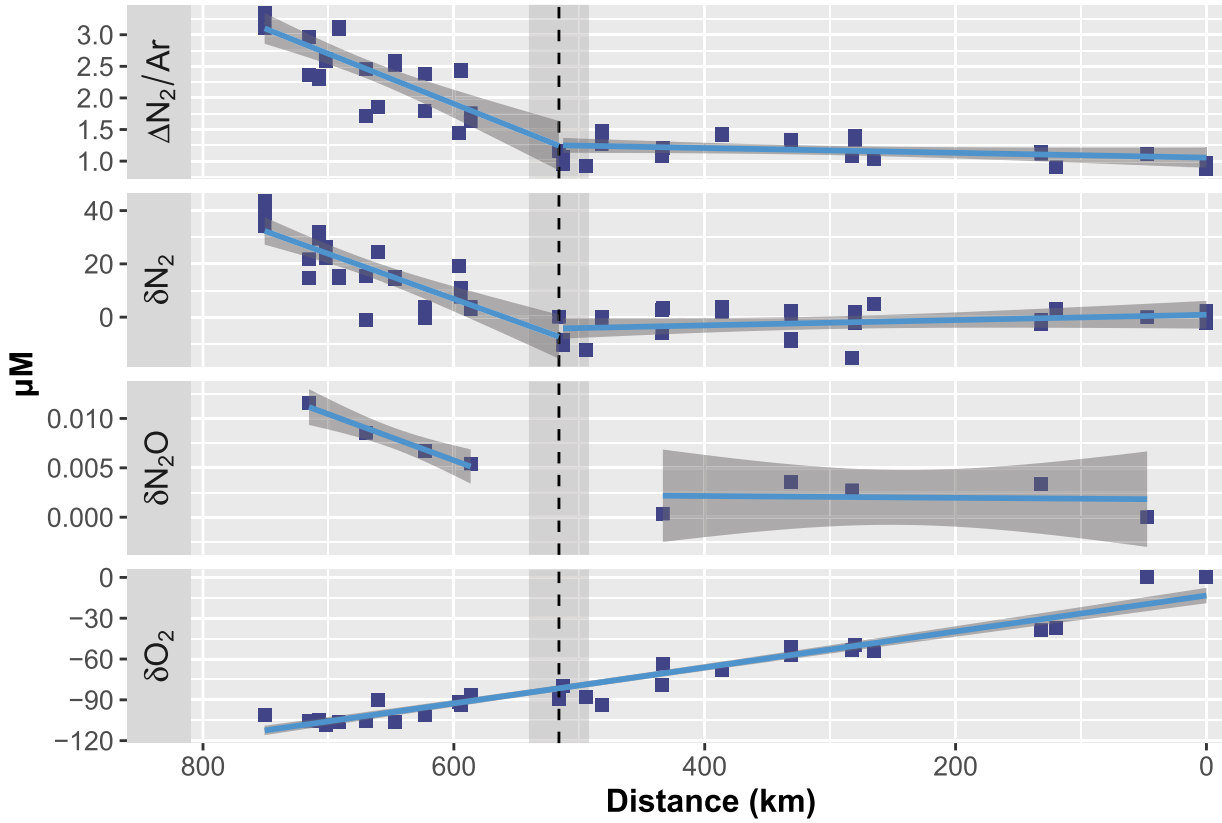

Figure 2. Bottom water gas concentration changes along the Laurentian Channel. Compilation (2021–2022–2023) of bottom water N_2/Ar supersaturation ratio ($\Delta N_2/Ar$) and standardized N_2 (δN_2), N_2O (δN_2O) and O_2 (δO_2) concentrations along the Laurentian Channel. The blue lines depict the linear models and associated errors (dark gray shades). The dashed vertical line depicts the location of the breakpoint, and its associated uncertainty (light gray shades) computed from $\Delta N_2/Ar$ data. The km 0 corresponds to station 1, which represents the easternmost point of the segment above the [O_2] threshold. All δ values are calculated relative to station 1.

associated with this breakpoint was 58.9 ± 1.1 μM. $\Delta N_2/Ar$ was relatively constant in the segment above the [O_2] threshold and increased significantly in the segment below the [O_2] threshold (Table 1). δN_2 and δN_2O followed the same pattern with relatively constant values in the segment above the [O_2] threshold, resulting in a J_{net} value not significantly different than zero (Table 1), and then linearly increased in the segment below the [O_2] threshold, resulting in significant positive value for J_{net} (Table 1). In contrast, δO_2 linearly decreased all along the LC (Table 1).

3.2. Bottom Water Nutrient Concentrations

Along the LC, the concentration of NO_3^- in bottom waters increased slightly in the segment above the [O_2] threshold, although the change was not significant, and decrease in the segment below the [O_2] threshold. The result was a trend toward net NO_3^- production in the segment above the [O_2] threshold and net NO_3^- consumption in the segment below the [O_2] threshold (Figure 3 and Table 1). PO_4^{3-} concentrations in the bottom water increased in the segment above the [O_2] threshold and this increase became more pronounced in the segment below the [O_2] threshold, indicating significant net production of PO_4^{3-} in both segments, with higher rate below the [O_2] threshold. N^* was stable in the segment above the [O_2] threshold and significantly decreased in the segment below the [O_2] threshold.

3.3. Pore Water Solute Concentrations and Benthic Fluxes

Oxygen micro-electrode profiles indicated a O_2 penetration depth of 1.86 ± 0.07 and 1.42 ± 0.04 cm at stations 17 and 28 respectively and associated diffusive fluxes (J_{diff}) of 2.08 ± 0.05 and 2.06 ± 0.12 mmol m^{-2} d^{-1} (Figures 4 and 5). The pore water NO_3^- profiles were characterized by a sharp decrease of concentration from the sediment-water interface down to 2–3 cm depth, where NO_3^- concentrations were near the detection limit (except for a peak

Table 1
Statistical Results

	Above $[O_2]$ threshold						Below $[O_2]$ threshold					
Variable	Slope	SE	t value	p value	Adj. R^2	J_{net}	Slope	SE	t value	p value	Adj. R^2	J_{net}
Gas												
$\Delta N_2/Ar$	0.0004	0.0002	1.71	0.102	0.08	–	0.0079	0.0011	6.88	**<0.001**	0.65	–
δN_2	−0.0100	0.0072	−1.38	0.181	0.04	−1.6	0.1690	0.0241	6.98	**<0.001**	0.66	26.7
δN_2O	0.0009	0.0063	0.14	0.895	−0.32	0.1	0.0467	0.0051	9.13	**0.012**	0.96	7.4
δO_2	−0.1321	0.0052	−25.46	**<0.001**	0.93	−20.8	–	–	–	–	–	–
Nutrients												
NO_3^-	0.0055	0.0028	1.99	0.067	0.16	0.9	−0.0163	0.0074	−2.21	**0.045**	0.20	−2.6
PO_4^{3-}	0.0004	0.0001	2.93	**0.011**	0.34	0.1	0.0024	0.0008	3.01	**0.009**	0.35	0.4
N*	−0.0010	0.0041	−0.23	0.821	−0.07	−0.2	−0.0553	0.0166	−3.33	**0.005**	0.40	−8.7

Note. Results of linear models on the relationship between the distance along the Laurentian Channel and (i) gas (i.e., $\Delta N_2/Ar$, δN_2, δN_2O, δO_2) and (ii) nutrients (i.e., NO_3^-, PO_4^{3-}, and N*) and associated J_{net} values (in mmol m^{-3} y^{-1}, except δN_2O in µmol m^{-3} y^{-1}) in the segment above (0–516.2 km) and below (516.2–750.9 km) the $[O_2]$ threshold. Values in bold indicate significant (p value <0.05) slopes. Please note that only one model output is provided for δO_2 due to its linear relationship with the distance along the Laurentian Channel.

at 6 cm at station 17). The NO_3^- concentration immediately below the sediment-water interface was higher at station 17 than station 28, resulting in a larger diffusive flux into the sediment at station 28 than station 17 (−626.45 vs. −431.23 µmol m^{-2} d^{-1}, respectively). The pore water NO_2^- profiles followed the same pattern as the NO_3^- although the concentration was one order of magnitude lower for NO_2^-. The pore water NH_4^+ profiles showed an increase of concentration with depth. At station 17, this increase was (quasi) linear from the sediment

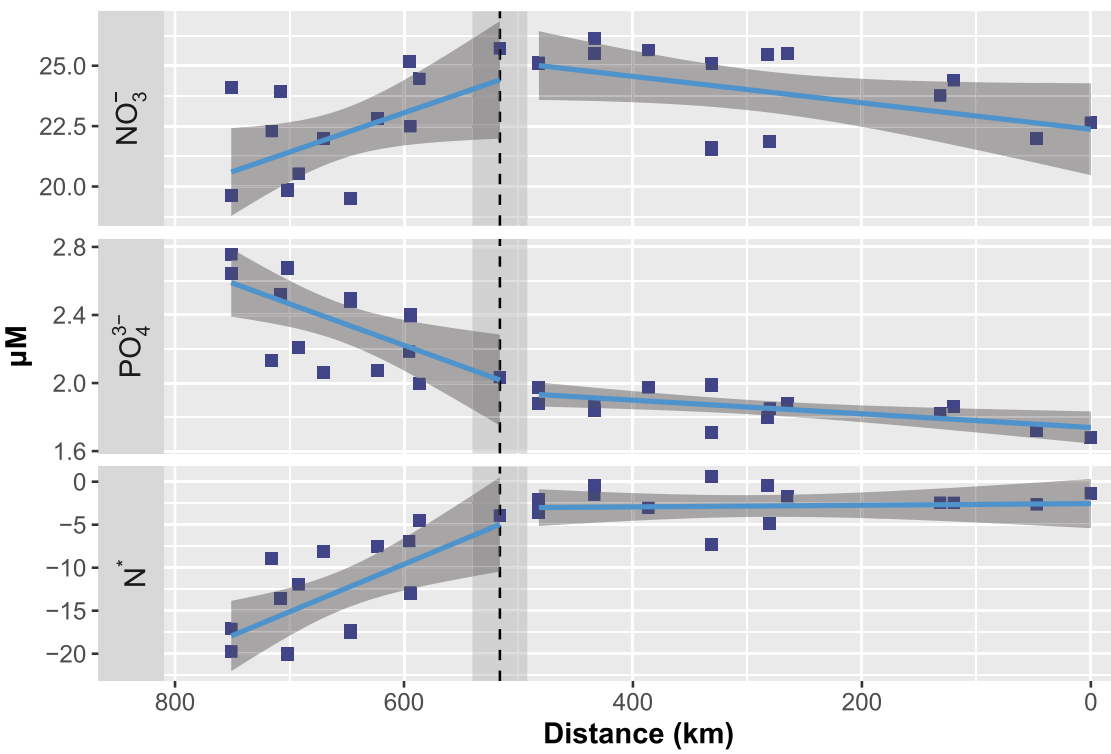

Figure 3. Bottom water nutrient concentration changes along the Laurentian Channel. The blue lines depict the linear models and their associated errors (dark gray shades). The dashed vertical line depicts the location of the breakpoint, and its associated uncertainty (light gray shades) computed from $\Delta N_2/Ar$ data. The km 0 corresponds to station 1, which represents the easternmost point of the segment above the $[O_2]$ threshold.

10.1029/2024GB008218

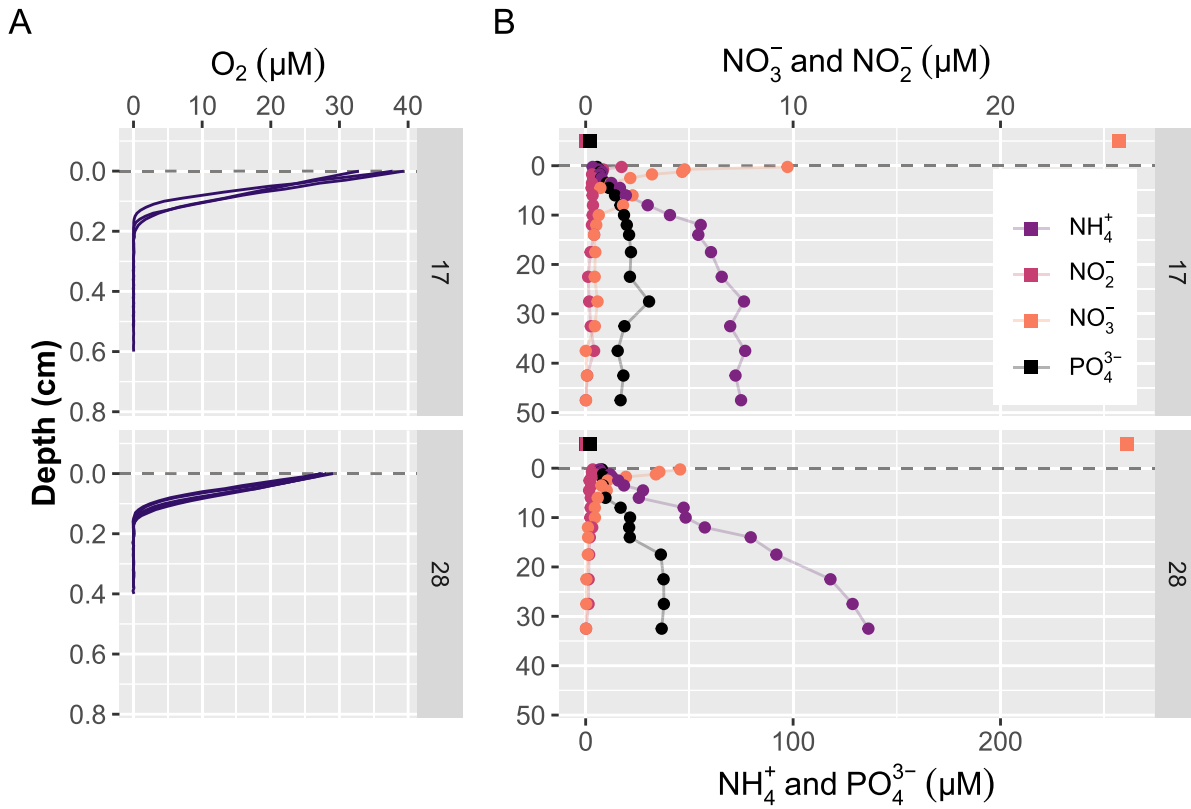

Figure 4. Pore water solute concentrations. Vertical depth profiles of (a) O_2 and (b) NO_2^-, NO_3^- PO_4^{3-} and NH_4^+ in the sediment column at stations 17 and 28 in 2021. (b) Squares indicate solute concentration in the bottom waters. Please note the *y* scale change between panels (a and b) and the presence of different *x* scales in panel (b).

surface to 27.5 cm and then the NH_4^+ concentration remained relatively constant around 75 μM until the bottom of the core. At station 28, the NH_4^+ concentration increased linearly with depth and exceeded 135 μM at the bottom of the core. At both stations, NH_4^+ was detectable in the first mm of the sediment column with concentrations higher than those in the overlying water, resulting in diffusive fluxes of 5.73 and 19.47 μmol m^{-2} d^{-1} toward the water column at station 17 and 28, respectively. The pore water PO_4^{3-} profiles showed an increase of concentration with depth. At station 17, the PO_4^{3-} concentration increases from the surface sediment to 10 cm and then remains relatively constant around 20 μM until the bottom of the core. At station 28, the PO_4^{3-} concentration increases from the surface sediment to 10 cm, remained relatively constant around 20 μM until 15 cm and then increased to reach 35 μM until the bottom of the core.

NH_4^+ and PO_4^{3-} benthic fluxes were barely detectable and did not show significant difference between stations (Figure 5a and Table 2). O_2 and NO_3^- were both consumed by the sediment and showed significant differences between stations. Indeed, station 17 showed larger O_2 and lower NO_3^- fluxes than station 28. Overall, total benthic fluxes were mostly driven by diffusive fluxes, as suggested by the similarity between the calculated diffusive fluxes and the total measured fluxes. Because of relatively high variability (especially at station 17), there was no significant difference (Table 2) in total denitrification rates (D_{tot}) between stations 17 and 28. However, D_{tot} tended to be lower at station 17 than at station 28 (288.59 ± 92.39 vs. 455.53 ± 29.46 μmol m^{-2} d^{-1}; Figure 5). The proportion of denitrification of NO_3^- produced through nitrification in the sediment (i.e., coupled nitrification-denitrification, D_n) was larger at station 17 than 28 (Figure 5). DNRA (data not shown) was not detected and, as mentioned in the methods section, was therefore not considered significant.

4. Discussion

The Estuary and Gulf of St. Lawrence (EGSL) has been subject to persistent hypoxic conditions since the 1980s with bottom water oxygen concentration around 60 μM (Gilbert et al., 2005). Since then, nitrogen cycling in the

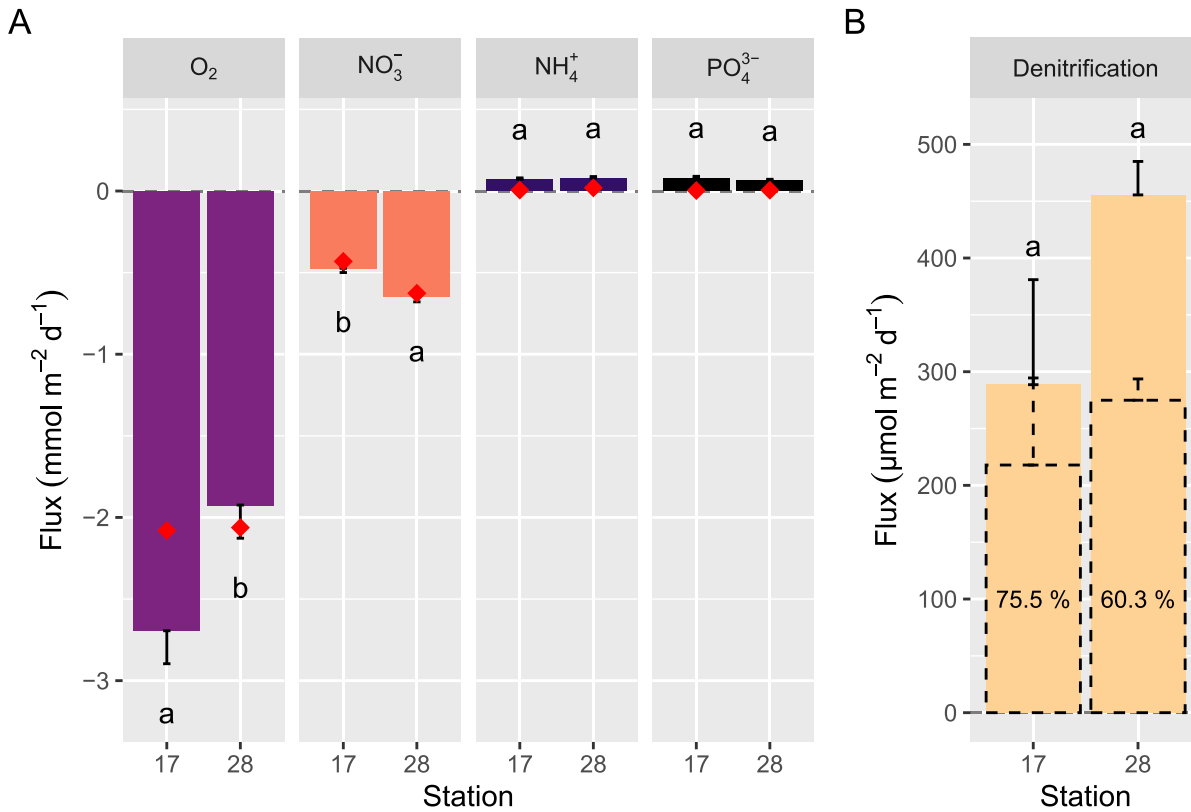

Figure 5. Benthic fluxes. (a) Mean ± SE total benthic fluxes ($J_{benthic}$) of O_2, NO_3^-, and NH_4^+ (mmol m^{-2} hr^{-1}) and (b) potential denitrification rates (D_{tot} in μmol m^{-2} hr^{-1}) at stations 17 and 28 in 2021. The red diamonds (a) depict the diffusive fluxes for each element. Dashed bar plots (b) depict the denitrification of nitrate produced within the sediment through nitrification (D_n) and the percentage represents the proportion of D_{tot} explained by D_n. Please note that NO_2^- fluxes are not depicted because NO_2^- concentrations in the overlying water of incubators were below the quantification limit. Different letters indicate significant ($p < 0.05$) differences between stations.

EGSL has been studied twice at the minimum O_2 concentration area (i.e., station 28) using ex situ isotope pairing experiment (Crowe et al., 2012) and at the regional scale using N^* along the LC (Thibodeau et al., 2010). However, both the extent and the severity of hypoxia in the EGSL have dramatically increased since 2020 (Jutras, Mucci, et al., 2023). This drastic drop in oxygen concentration gives a unique opportunity to assess the influence of decreasing oxygen concentration on nitrogen cycling in the natural environment. Here we combine measurement of N_2/Ar, N_2O and N^* tracers that integrate fixed-nitrogen removal processes over large spatial scales with sediment core incubations conducted at two specific stations to gain insight on the processes contributing to N_2 production in the bottom water of the EGSL.

Table 2
Statistical Results

Variable	Source	Df	SS	*F*	*p* value
O_2	Station	1	1.779	7.224	**0.023**
	Residuals	10	2.463	–	–
NO_3^-	Station	1	0.088	15.308	**0.003**
	Residuals	10	0.057	–	–
NH_4^+	Station	1	0.000	0.135	0.721
	Residuals	10	0.006	–	–
PO_4^{3-}	Station	1	0.001	1.253	0.289
	Residuals	10	0.006	–	–
D_{tot}	Station	1	0.056	2.964	0.136
	Residuals	6	0.113	--	--

Note. Results of ANOVA test on the effect of Station on benthic fluxes. Values in bold indicate significant ($p < 0.05$) differences between stations.

4.1. Signals of Fixed-Nitrogen Removal Processes in Bottom Waters Along the LC

Our results show a segmented linear relationship between nitrogen cycling tracers (i.e., N_2/Ar, N_2, and N^*) and the distance along the LC with a breakpoint located at km 516 (Figures 2 and 3). In the segment above the [O_2] threshold (to the east of the breakpoint), N_2 and N_2O concentrations are stable suggesting that processes consuming and producing those gases are either absent or offset each other. In the segment below the [O_2] threshold (to the west of the breakpoint), in bottom waters characterized by O_2 concentrations below 58.9 ± 1.1 μM, we observed accumulation of both N_2 and N_2O in the bottom water. The increase in N_2 and N_2O in the bottom water is linear, rather

than exponential, suggesting that decreasing O_2 concentrations expand the spatial extent of fixed-nitrogen removal without accelerating N_2 and N_2O production rates over the examined oxygen range. As shown by our water mixing analysis (see Supporting Information S1), this accumulation cannot be explained by mixing with more surficial waters, which accounted for less than 10% of the observed signal. This suggests that deoxygenation enables the activation of these processes across broader areas, rather than intensifying them within localized regions. Therefore, the breakpoint identified here should not be regarded as a static location, as it may shift eastward with the expansion of the area characterized by O_2 concentration below the identified threshold (or vice versa). Notably, the accumulation of N_2 and N_2O co-occurred with a decrease in N^*, implying a significant role of fixed-nitrogen removal processes in shaping the N:P ratio in the bottom waters of the EGSL. A severe nitrogen deficit had already been observed in the hypoxic bottom waters of the EGSL in 2006, without the mechanisms behind the deficit being determined (Thibodeau et al., 2010). We observed an even stronger nitrogen deficit signal, with N^* values as low as −20.1 μM, compared to the minimum of −11 μM in 2006 reported by Thibodeau et al. (2010). This discrepancy is not attributable to inter-annual variability since N^* values computed from historical data from 2006 to 2023 (DFO, 2024) show relatively stable nitrate deficit over this period, with a marked increase of this deficit beginning in 2020 (Figure S5 in Supporting Information S1). Interestingly, this decline aligns with the findings of Jutras, Mucci, et al. (2023), who reported a sharp decrease in oxygen concentration in 2020 when minimum levels dropped from 60–55 to 35 μM, which is consistent with the $[O_2]$ threshold found in the present study. This decrease was associated with an expansion of hypoxic zones from ∼1,300 in 2003 to ∼9,400 km^2 (Jutras, Mucci, et al., 2023). This points toward an intensification of fixed-nitrogen removal processes over the past 16 years. This intensification was not linear and probably started in 2020.

4.2. Sedimentary Pathways and Benthic Rates of Fixed-Nitrogen Removal Processes

While Crowe et al. (2012) showed that anammox could occur in the sediment of the LC, the resulting concentration of the $^{15}N - NO_3^-$ tracer added in the overlying water of their incubated sediment cores was an order of magnitude higher than the natural concentrations, and thus substantially above the levels used in the present study. Such a high amendment may artificially increase anammox rates (Risgaard-Petersen et al., 2003). Although their results indicate that environmental conditions could support anammox in the sediment of the Laurentian Channel, we suggest that their experimental design does not provide conclusive evidence that anammox occurs at significant rates under in situ conditions. In this study, we used the original IPT, which does not distinguish anammox from denitrification. Although we checked for the validity of the original IPT (including the hypothesis of absence of anammox), it is possible that our sampling strategy did not capture the spatial variability of nitrogen processes in the sediment and failed to detect localized anammox process (Risgaard-Petersen et al., 2003). If anammox contributes significantly to N_2 production, then our estimated benthic N_2 fluxes would be overestimated (Risgaard-Petersen et al., 2003). In that case, the contribution of sedimentary fluxes to fixed-nitrogen loss would also be overestimated in our partitioning framework. Regardless of the specific mechanisms responsible for N_2 production, our results are consistent with the previously reported N_2 production rates ranging from 403 to 640 μmol m^{-2} d^{-1} (Crowe et al., 2012; Katsev et al., 2007; Thibodeau et al., 2010), even though bottom water O_2 concentrations have significantly dropped since the earlier studies were conducted (ranging from ∼63 to 34.6 μM). These results suggest that, within the range of studied conditions, rates of benthic N_2 production are not related to bottom water O_2 concentration. The comparison of stations 17 and 28, with contrasted bottom water O_2 concentration, reveals however a reduced sedimentary nitrification contribution to denitrification as bottom water O_2 decreases. Bioturbation is recognized for its role in enhancing nitrification-denitrification processes (Stief, 2013). However, recent findings by Pascal et al. (2023) indicated negligible bioturbation rates below an O_2 concentration of *ca*. 63 μM in the EGSL. In hypoxic conditions and in the absence of bioturbation, O_2 is anticipated to quickly become a limiting factor for sedimentary nitrification. Consequently, sedimentary denitrification is expected to draw more nitrate from the water column, which aligns with the patterns observed in our benthic flux and pore water data.

4.3. Partitioning Fixed-Nitrogen Removal Processes

In our conceptual model, we attribute changes in gas composition in the water column (J_{net}) to either water column (J_w) or benthic ($J_{benthic}$) processes. By incorporating J_{net}, $J_{benthic}$ and the water column height of our conceptual model ($z = 118.32$ m), we can calculate J_w, enabling us to allocate fixed-nitrogen removal processes in both the water column and the sediment, specifically in the segment below the $[O_2]$ threshold. In this segment, J_w

ranged between 25.80 and 25.30 mmol m^{-3} y^{-1} corresponding to 96.70% to 94.70% of J_{net}. We acknowledge that this is a rough estimate, and our model limitations and uncertainties are described above (see Section 2.6.2). However, the vertical diffusivity in the bottom waters of the EGSL was estimated to be of the order of 10^{-6} (Cyr et al., 2011) to 10^{-5} m^2 s^{-1} (Stevens et al., 2024), which is insufficient to account for transport over more than 100 m, as observed in Figure S6 in Supporting Information S1. In addition, we conducted a sensitivity analysis by reducing the net bottom water flow by a factor of 3 and a potential mixing at the head of the Laurentian Channel to simulate local current potentially affecting bottom water flow, as detailed in Section 2.6.2 and Supporting Information S1. This analysis demonstrated that even under such conditions, our main conclusions remained robust. Therefore, our findings suggest that water column fixed-nitrogen removal processes likely contribute to the observed N_2 production. To confirm these findings, future studies should incorporate direct measurements of water column denitrification. N_2/Ar and benthic flux measurements integrate processes over different spatial and temporal scales. While combining these approaches provides complementary insights, further research is needed to better constrain the spatial and temporal variability of benthic N_2 fluxes. This will enable a more accurate assessment of their contribution to bottom water N_2 accumulation and provide a more comprehensive understanding of nitrogen cycling in benthic environments.

Despite persistent hypoxic conditions, the O_2 concentration in the bottom water of the EGSL remains relatively high (>32 μM) which raises questions about the mechanisms sustaining anaerobic fixed-nitrogen removal processes. Laboratory and modeling studies suggest that these processes can occur within microenvironments of the water column, such as suspended particles or marine snow (Alldredge & Cohen, 1987; Bianchi et al., 2018; Ciccarese et al., 2023; Smriga et al., 2021; Stief et al., 2016, 2017), and may significantly contribute to total N_2 production. In addition, the sedimentation rate is relatively high in the hypoxic area (Audet et al., 2023; Smith & Schafer, 1999), which may contribute to an increase in the quantity of microenvironment in the water column where fixed-nitrogen removal processes can occur. Interestingly, Lévesque et al. (2023) found a decrease in total OM in the deep waters of the Lower St. Lawrence Estuary as compared to the intermediate waters, suggesting that significant OM mineralization occurs in this hypoxic area. In addition to O_2 concentration, the quantity and the quality of organic matter likely play a crucial role in driving fixed-nitrogen removal processes. The observed O_2 threshold for N_2 (and N_2O) production reflects the combined influence of decreasing ambient O_2 concentration and the characteristics of (re)suspended organic matter, which together promote the formation of microenvironments where local O_2 concentrations can drop below the suboxia (<5 μM) thresholds, allowing fixed-nitrogen removal to become the dominant process. Notably, N_2O can also be produced via nitrification and often peaks under hypoxic conditions, indicating that its production is not strictly limited to suboxic environment. Therefore, assessing potential areas for fixed-nitrogen removal in the ocean requires considering not only oxygen levels but also the availability and quality of (re)suspended organic matter.

4.4. Broader Implications

The possibility that fixed-nitrogen removal processes can occur even when ambient water column O_2 concentrations exceed the commonly used suboxic threshold (<5 μM) may have significant implications for our understanding of marine nitrogen cycling. Our results are consistent with the hypothesis that microenvironments within (re)suspended organic matter may locally achieve suboxic conditions favorable for these processes, even when the surrounding water column oxygen measurements are above threshold values. This suggests that water column oxygen concentration alone does not always be a sufficient proxy for identifying all zones of fixed-nitrogen removal in marine systems. This hypothesis highlights the need for direct measurements of fixed-nitrogen removal processes in hypoxic water columns.

In coastal systems like the Lower St. Lawrence Estuary, where bottom waters can supply up to 60% of surface nutrients (Jutras, Mucci, et al., 2020), the removal of fixed nitrogen may reduce surface productivity. As bioavailable nitrogen is lost from the water column, surface waters may become increasingly nitrogen-limited, potentially altering phytoplankton growth and community structure (Hecky & Kilham, 1988). Nitrate limitation has been shown to favor communities dominated by small cells with low production (Lee et al., 2013; W. K. W. Li et al., 2009; Mills et al., 2018; Moore et al., 2013). A reduced N:P ratio, reflecting excess of phosphate, has also been observed in other hypoxic systems such as the Chesapeake Bay and the Baltic Sea, where summer stratification coupled with oxygen depletion enhances the availability of dissolved inorganic phosphate while dissolved inorganic nitrogen is lost through denitrification (Kuliński et al., 2022; J. Li et al., 2017). In the Baltic Sea, such conditions have promoted nitrogen-fixing cyanobacteria, altering community structure and the stoichiometry of

organic matter production (Munkes et al., 2021). These shifts in phytoplankton composition can significantly impact both the quality and quantity of exported organic material, cascading through the food web and ultimately affecting higher trophic levels (Kwiatkowski et al., 2019).

We also report evidence for N_2O production in the hypoxic area, raising questions about its production mechanisms and fate. N_2O is produced as a byproduct of both nitrification and denitrification pathways, with their relative contributions and production yields modulated by ambient oxygen concentrations (Ji et al., 2018). Peak in N_2O production typically occurs at low oxygen concentrations within the oxycline of oxygen minimum zones (Frey et al., 2020; Ji et al., 2018). In the Baltic Sea, N_2O accumulation in the water column begins when O_2 concentrations fall below 50 to 20 μM (Walter et al., 2006). Similar observations have been made in the Chesapeake Bay (Tang et al., 2022) and the Gulf of Mexico (Naqvi et al., 2010). In addition to low O_2, sediment resuspension enhances N_2O production, particularly under hypoxic conditions (Liu et al., 2024). In our study, the observed increase in N_2O in bottom waters across the hypoxic segment likely results from the combined effects of low O_2 and sediment resuspension. Upwelling of these N_2O-rich bottom waters may contribute to atmospheric emission of this potent greenhouse gas, potentially creating positive feedback on climate change. Further investigation is needed to determine whether these bottom waters reach the surface and release N_2O to the atmosphere.

This study emphasizes the importance of better understanding the multifaceted impacts of ocean deoxygenation, not only in the Estuary and Gulf of St. Lawrence but also in other marine environments susceptible to oxygen depletion. Our findings may help inform the study of similar processes in diverse coastal and oceanic systems worldwide experiencing deoxygenation. Importantly, our research highlights key uncertainties regarding biogeochemical feedbacks, ecosystem impacts, and global GHG budgets, emphasizing the need for comparative studies across different systems. As oxygen minimum zones expand in coastal and oceanic areas (Breitburg et al., 2018), deepening our understanding of these complex processes becomes increasingly pressing.

Data Availability Statement

The 2021, 2022, and 2023 data sets and R code used in this study are available at St. Lawrence Global Observatory (SLGO) via https://doi.org/10.26071/ogsl-abd9c822-1ade with CC-BY 4.0 (Pascal et al., 2025). The BioChem database from the Department of Ficheries and Oceans Canada can be accessed at https://www.dfo-mpo.gc.ca/science/data-donnees/biochem/index-eng.html.

Acknowledgments
We thank the captain and the crew of the R/V Coriolis II for their expert assistance at sea and their dedication. We acknowledge the help of Olivier Herard and William Nesbitt in coordinating some of the sampling at sea and data curation. We also thank Alfonso Mucci for providing the equipment and its assistance in porewater sampling. We would like to extend our warm thanks to Marjolaine Blais for granting us the opportunity to collect water samples during the Atlantic Zone Monitoring Program (AZMP) campaigns of DFO Canada and André Pellerin for granting us the opportunity to conduct high-resolution water column sampling during his dedicated ship time. We thank DFO Canada for providing access to the historical nutrient data. We are grateful to the three anonymous reviewers, the associate editor, and the editor-in-chief for their thorough work and significant contributions to improving the manuscript. LP is grateful to Sophie Moisset for her moral support. Ship time was funded by Natural Sciences and Engineering Research Council of Canada (NSERC) ship time program to GC (556538-2021-RGPST), the Marine Environmental Observation, Prediction and Response Network (MEOPAR), the "programme Odyssée Saint Laurent" from the "Réseau Québec maritime" (RQM) and the programme PLAINE funded by the government of Québec and coordinated by the RQM. LP was supported by a postdoctoral fellowship from MEOPAR (#PDF-25-2020) and B3X postdoctoral fellowships from FRQNT (281864; https://doi.org/10.69777/281864 and 322485; https://doi.org/10.69777/322485). GC is supported by NSERC discovery grant (RGPIN-2018-556538).

References

Alldredge, A. L., & Cohen, Y. (1987). Can microscale chemical patches persist in the sea? Microelectrode study of marine snow, Fecal Pellets. *Science*, *235*(4789), 689–691. https://doi.org/10.1126/science.235.4789.689

Aminot, A., Kérouel, R., & Coverly, S. C. (2009). Nutrients in seawater using segmented flow analysis. In *Practical guidelines for the analysis of seawater* (p. 408). CRC Press. https://doi.org/10.1201/9781420073072

Audet, T., de Vernal, A., Mucci, A., Seidenkrantz, M.-S., Hillaire-Marcel, C., Carnero-Bravo, V., & Gélinas, Y. (2023). Benthic foraminiferal assemblages from the Laurentian Channel in the Lower Estuary and Gulf of ST. Lawrence, Eastern Canada: Tracers of bottom-water hypoxia. *Journal of Foraminiferal Research*, *53*(1), 57–77. https://doi.org/10.2113/gsjfr.53.1.57

Bianchi, D., Weber, T. S., Kiko, R., & Deutsch, C. (2018). Global niche of marine anaerobic metabolisms expanded by particle microenvironments. *Nature Geoscience*, *11*(4), 263–268. https://doi.org/10.1038/s41561-018-0081-0

Bluteau, C. E., Galbraith, P. S., Bourgault, D., Villeneuve, V., & Tremblay, J.-É. (2021). Winter observations alter the seasonal perspectives of the nutrient transport pathways into the lower St. Lawrence Estuary. *Ocean Science*, *17*(5), 1509–1525. https://doi.org/10.5194/os-17-1509-2021

Bonin, P., Gilewicz, M., & Bertrand, J. C. (1989). Effects of oxygen on each step of denitrification on *Pseudomonas nautica*. *Canadian Journal of Microbiology*, *35*(11), 1061–1064. https://doi.org/10.1139/m89-177

Bourgault, D., Cyr, F., Galbraith, P. S., & Pelletier, E. (2012). Relative importance of pelagic and sediment respiration in causing hypoxia in a deep estuary. *Journal of Geophysical Research*, *117*(C8), 2012JC007902. https://doi.org/10.1029/2012JC007902

Bowen, J. L., Giblin, A. E., Murphy, A. E., Bulseco, A. N., Deegan, L. A., Johnson, D. S., et al. (2020). Not all nitrogen is created equal: Differential effects of nitrate and ammonium enrichment in coastal wetlands. *BioScience*, *70*(12), 1108–1119. https://doi.org/10.1093/biosci/biaa140

Breitburg, D., Levin, L. A., Oschlies, A., Grégoire, M., Chavez, F. P., Conley, D. J., et al. (2018). Declining oxygen in the global ocean and coastal waters. *Science*, *359*(6371), eaam7240. https://doi.org/10.1126/science.aam7240

Bugden, G. L. (1991). Changes in the temperature-salinity characteristics of the deeper waters of the Gulf of St. Lawrence over the past several decades. In *Gulf of St. Lawrence: Small oceanor big estuary?* (Vol. 113, pp. 139–147). Canadian Special Publication of Fisheries and Aquatic Sciences. Retrieved from https://waves-vagues.dfo-mpo.gc.ca/library-bibliotheque/20971_1.pdf

Ciccarese, D., Tantawi, O., Zhang, I. H., Plata, D., & Babbin, A. R. (2023). Microscale dynamics promote segregated denitrification in diatom aggregates sinking slowly in bulk oxygenated seawater. *Communications Earth & Environment*, *4*(1), 1–13. https://doi.org/10.1038/s43247-023-00935-x

Codispoti, L. (2007). An oceanic fixed nitrogen sink exceeding 400 Tg N a^{-1} vs the concept of homeostasis in the fixed-nitrogen inventory. *Biogeosciences*, *4*(2), 233–253. https://doi.org/10.5194/BG-4-233-2007

Crowe, S. A., Canfield, D. E., Mucci, A., Sundby, B., & Maranger, R. (2012). Anammox, denitrification and fixed-nitrogen removal in sediments from the Lower St. Lawrence Estuary. *Biogeosciences*, *9*(11), 4309–4321. https://doi.org/10.5194/bg-9-4309-2012

Cyr, F., Bourgault, D., & Galbraith, P. S. (2011). Interior versus boundary mixing of a cold intermediate layer. *Journal of Geophysical Research*, *116*(C12), C12029. https://doi.org/10.1029/2011JC007359

Cyr, F., Bourgault, D., Galbraith, P. S., & Gosselin, M. (2015). Turbulent nitrate fluxes in the Lower St. Lawrence Estuary, Canada. *Journal of Geophysical Research: Oceans*, *120*(3), 2308–2330. https://doi.org/10.1002/2014JC010272

Davies, R. B. (2002). Hypothesis testing when a nuisance parameter is present only under the alternative: Linear model case. *Biometrika*, *89*(2), 484–489. https://doi.org/10.1093/biomet/89.2.484

Deflandre, B., & Duchêne, J.-C. (2010). PRO2FLUX – A software program for profile quantification and diffusive O_2 flux calculations. *Environmental Modelling and Software*, *25*(9), 1059–1061. https://doi.org/10.1016/j.envsoft.2009.10.015

Devol, A. H. (2015). Denitrification, anammox, and N_2 production in marine sediments. *Annual Review of Marine Science*, *7*(1), 403–423. https://doi.org/10.1146/annurev-marine-010213-135040

DeVries, T., Deutsch, C., Primeau, F., Chang, B. X., & Devol, A. H. (2012). Global rates of water-column denitrification derived from nitrogen gas measurements. *Nature Geoscience*, *5*(8), 547–550. https://doi.org/10.1038/NGEO1515

DFO. (2024). BioChem: Database of biological and chemical oceanographic data [Dataset]. *Department of Fisheries and Oceans, Canada*. Retrieved from https://www.dfo-mpo.gc.ca/science/data-donnees/biochem/index-eng.html

Eyre, B. D., Rysgaard, S., Dalsgaard, T., & Christensen, P. B. (2002). Comparison of isotope pairing and N_2:Ar methods for measuring sediment denitrification—Assumption, modifications, and implications. *Estuaries*, *25*(6), 1077–1087. https://doi.org/10.1007/BF02692205

Frey, C., Bange, H. W., Achterberg, E. P., Jayakumar, A., Löscher, C. R., Arévalo-Martínez, D. L., et al. (2020). Regulation of nitrous oxide production in low-oxygen waters off the coast of Peru. *Biogeosciences*, *17*(8), 2263–2287. https://doi.org/10.5194/bg-17-2263-2020

Galbraith, P. S., Chassé, J., Shaw, J.-L., Dumas, J., & Bourassa, M.-N. (2024). *Physical oceanographic conditions in the Gulf of St. Lawrence in 2023* (Series No. 378) (p. 91). Department of Fisheries and Oceans, issuing body. Retrieved from https://publications.gc.ca/site/eng/9.938387/publication.html

Gilbert, D. (2004). Propagation of temperature signals from the northwest Atlantic continental shelf edge into the Laurentian Channel. *ICES CM*, N-7.

Gilbert, D., Sundby, B., Gobeil, C., Mucci, A., & Tremblay, G.-H. (2005). A seventy-two-year record of diminishing deep-water oxygen in the St. Lawrence estuary: The northwest Atlantic connection. *Limnology and Oceanography*, *50*(5), 1654–1666. https://doi.org/10.4319/lo.2005.50.5.1654

Grasshoff, K., Ehrhardt, M., & Kremling, K. (1999). Methods of seawater analysis.

Gruber, N., & Sarmiento, J. L. (1997). Global patterns of marine nitrogen fixation and denitrification. *Global Biogeochemical Cycles*, *11*(2), 235–266. https://doi.org/10.1029/97GB00077

Haas, S., Desai, D. K., LaRoche, J., Pawlowicz, R., & Wallace, D. W. R. (2019). Geomicrobiology of the carbon, nitrogen and sulphur cycles in Powell Lake: A permanently stratified water column containing ancient seawater. *Environmental Microbiology*, *21*(10), 3927–3952. https://doi.org/10.1111/1462-2920.14743

Hamme, R. C., & Emerson, S. R. (2004). The solubility of neon, nitrogen and argon in distilled water and seawater. *Deep Sea Research Part I: Oceanographic Research Papers*, *51*(11), 1517–1528. https://doi.org/10.1016/j.dsr.2004.06.009

Hamme, R. C., & Emerson, S. R. (2013). Deep-sea nutrient loss inferred from the marine dissolved N_2/Ar ratio. *Geophysical Research Letters*, *40*(6), 1149–1153. https://doi.org/10.1002/grl.50275

Hardison, A. K., Algar, C. K., Giblin, A. E., & Rich, J. J. (2015). Influence of organic carbon and nitrate loading on partitioning between dissimilatory nitrate reduction to ammonium (DNRA) and N_2 production. *Geochimica et Cosmochimica Acta*, *164*, 146–160. https://doi.org/10.1016/j.gca.2015.04.049

Hecky, R. E., & Kilham, P. (1988). Nutrient limitation of phytoplankton in freshwater and marine environments: A review of recent evidence on the effects of enrichment. *Limnology and Oceanography*, *33*(4part2), 796–822. https://doi.org/10.4319/lo.1988.33.4part2.0796

Hutchins, D. A., & Capone, D. G. (2022). The marine nitrogen cycle: New developments and global change. *Nature Reviews Microbiology*, *20*(7), 401–414. https://doi.org/10.1038/s41579-022-00687-z

Ji, Q., Buitenhuis, E., Suntharalingam, P., Sarmiento, J. L., & Ward, B. B. (2018). Global nitrous oxide production determined by oxygen sensitivity of nitrification and denitrification. *Global Biogeochemical Cycles*, *32*(12), 1790–1802. https://doi.org/10.1029/2018GB005887

Jutras, M., Dufour, C. O., Mucci, A., Cyr, F., & Gilbert, D. (2020). Temporal changes in the causes of the observed oxygen decline in the St. Lawrence Estuary. *Journal of Geophysical Research: Oceans*, *125*(12), e2020JC016577. https://doi.org/10.1029/2020JC016577

Jutras, M., Dufour, C. O., Mucci, A., & Talbot, L. C. (2023). Large-scale control of the retroflection of the Labrador Current. *Nature Communications*, *14*(1), 2623. https://doi.org/10.1038/s41467-023-38321-y

Jutras, M., Mucci, A., Chaillou, G., Nesbitt, W. A., & Wallace, D. W. R. (2023). Temporal and spatial evolution of bottom-water hypoxia in the St Lawrence estuarine system. *Biogeosciences*, *20*(4), 839–849. https://doi.org/10.5194/bg-20-839-2023

Jutras, M., Mucci, A., Sundby, B., Gratton, Y., & Katsev, S. (2020). Nutrient cycling in the Lower St. Lawrence Estuary: Response to environmental perturbations. *Estuarine, Coastal and Shelf Science*, *239*, 106715. https://doi.org/10.1016/j.ecss.2020.106715

Kana, T. M., Cornwell, J. C., & Zhong, L. (2006). Determination of denitrification in the Chesapeake Bay from measurements of N_2 accumulation in bottom water. *Estuaries and Coasts*, *29*(2), 222–231. https://doi.org/10.1007/BF02781991

Kana, T. M., Darkangelo, C., Hunt, M. D., Oldham, J. B., Bennett, G. E., & Cornwell, J. C. (1994). Membrane inlet mass spectrometer for rapid high-precision determination of N_2, O_2, and Ar in environmental water samples. *Analytical Chemistry*, *66*(23), 4166–4170. https://doi.org/10.1021/ac00095a009

Katsev, S., Chaillou, G., Sundby, B., & Mucci, A. (2007). Effects of progressive oxygen depletion on sediment diagenesis and fluxes: A model for the lower St. Lawrence River Estuary. *Limnology and Oceanography*, *52*(6), 2555–2568. https://doi.org/10.4319/lo.2007.52.6.2555

Kelley, D., & Richards, C. (2022). oce: Analysis of oceanographic data. Retrieved from https://CRAN.R-project.org/package=oce

Koutitonsky, V., & Bugden, G. L. (1991). The physical oceanography of the Gulf of St. Lawrence: A review with emphasis on the synoptic variability of the motion. In J. C. Therriault (Ed.), *Gulf of St. Lawrence: Small oceanor big estuary?* (Vol. 113, pp. 57–90). Canadian Special Publication of Fisheries and Aquatic Sciences. Retrieved from https://waves-vagues.dfo-mpo.gc.ca/library-bibliotheque/20971_1.pdf

Kuliński, K., Rehder, G., Asmala, E., Bartosova, A., Carstensen, J., Gustafsson, B., et al. (2022). Biogeochemical functioning of the Baltic Sea. *Earth System Dynamics*, *13*(1), 633–685. https://doi.org/10.5194/esd-13-633-2022

Kwiatkowski, L., Aumont, O., & Bopp, L. (2019). Consistent trophic amplification of marine biomass declines under climate change. *Global Change Biology*, *25*(1), 218–229. https://doi.org/10.1111/gcb.14468

Lam, P., & Kuypers, M. M. M. (2011). Microbial nitrogen cycling processes in oxygen minimum zones. *Annual Review of Marine Science*, *3*(1), 317–345. https://doi.org/10.1146/annurev-marine-120709-142814

Lee, S. H., Sun Yun, M., Kyung Kim, B., Joo, H., Kang, S.-H., Keun Kang, C., & Whitledge, T. E. (2013). Contribution of small phytoplankton to total primary production in the Chukchi Sea. *Continental Shelf Research*, *68*, 43–50. https://doi.org/10.1016/j.csr.2013.08.008

Lévesque, D., Lebeuf, M., Maltais, D., Anderson, C., & Starr, M. (2023). Transport inventories and exchanges of organic matter throughout the St. Lawrence Estuary continuum (Canada). *Frontiers in Marine Science*, *9*, 1055384. https://doi.org/10.3389/fmars.2022.1055384

Li, J., Bai, Y., Bear, K., Joshi, S., & Jaisi, D. (2017). Phosphorus availability and turnover in the Chesapeake Bay: Insights from nutrient stoichiometry and phosphate oxygen isotope ratios. *Journal of Geophysical Research: Biogeosciences*, *122*(4), 811–824. https://doi.org/10.1002/2016JG003589

Li, W. K. W., McLaughlin, F. A., Lovejoy, C., & Carmack, E. C. (2009). Smallest algae thrive as the Arctic Ocean freshens. *Science*, *326*(5952), 539. https://doi.org/10.1126/science.1179798

Liu, S., Gao, Q., Wu, J., Xie, Y., Yang, Q., Wang, R., & Cui, Y. (2024). The concentration of CH_4, N_2O and CO_2 in the Pearl River estuary increased significantly due to the sediment particle resuspension and the interaction of hypoxia. *Science of the Total Environment*, *911*, 168795. https://doi.org/10.1016/j.scitotenv.2023.168795

Middelburg, J. J., & Levin, L. (2009). Coastal hypoxia and sediment biogeochemistry. *Biogeosciences*, *6*(7), 1273–1293. https://doi.org/10.5194/bg-6-1273-2009

Middelburg, J. J., Soetaert, K., Herman, P. M. J., & Heip, C. H. R. (1996). Denitrification in marine sediments: A model study. *Global Biogeochemical Cycles*, *10*(4), 661–673. https://doi.org/10.1029/96gb02562

Mills, M. M., Brown, Z. W., Laney, S. R., Ortega-Retuerta, E., Lowry, K. E., van Dijken, G. L., & Arrigo, K. R. (2018). Nitrogen limitation of the summer phytoplankton and heterotrophic prokaryote communities in the Chukchi Sea. *Frontiers in Marine Science*, *5*, 362. https://doi.org/10.3389/fmars.2018.00362

Moore, C. M., Mills, M. M., Arrigo, K. R., Berman-Frank, I., Bopp, L., Boyd, P. W., et al. (2013). Processes and patterns of oceanic nutrient limitation. *Nature Geoscience*, *6*(9), 701–710. https://doi.org/10.1038/ngeo1765

Muggeo, V. M. R. (2017). Interval estimation for the breakpoint in segmented regression: A smoothed score-based approach. *Australian and New Zealand Journal of Statistics*, *59*(3), 311–322. https://doi.org/10.1111/anzs.12200

Munkes, B., Löptien, U., & Dietze, H. (2021). Cyanobacteria blooms in the Baltic Sea: A review of models and facts. *Biogeosciences*, *18*(7), 2347–2378. https://doi.org/10.5194/bg-18-2347-2021

Naqvi, S. W. A., Bange, H. W., Farías, L., Monteiro, P. M. S., Scranton, M. I., & Zhang, J. (2010). Marine hypoxia/anoxia as a source of CH_4 and N_2O. *Biogeosciences*, *7*(7), 2159–2190. https://doi.org/10.5194/bg-7-2159-2010

Nielsen, L. P. (1992). Denitrification in sediment determined from nitrogen isotope pairing. *FEMS Microbiology Letters*, *86*(4), 357–362. https://doi.org/10.1111/j.1574-6968.1992.tb04828.x

Pascal, L., Cloutier-Artiwat, F., Wallace, D. W. R., & Chaillou, G. (2025). Exploring nitrogen cycling in oxygen-depleted oceans: Description from estuary and Gulf of St. Lawrence (Version 1) [Dataset]. *St. Lawrence Global Observatory*. https://doi.org/10.26071/ogsl-abd9c822-1ade

Pascal, L., Cool, J., Archambault, P., Calosi, P., Cuenca, A. L. R., Mucci, A. O., & Chaillou, G. (2023). Ocean deoxygenation caused non-linear responses in the structure and functioning of benthic ecosystems. *Global Change Biology*, *30*(1), e16994. https://doi.org/10.1111/gcb.16994

Petrie, B., Drinkwater, K., Sandstrom, A., Pettipas, R., Gregory, D., Gilbert, D., & Sekhon, P. (1996). Temperature, salinity and sigma-t atlas for the Gulf of St. Lawrence (Vol. *178*, p. 256). Retrieved from https://waves-vagues.dfo-mpo.gc.ca/library-bibliotheque/198079.pdf

Punshon, S., & Moore, R. M. (2004). Nitrous oxide production and consumption in a eutrophic coastal embayment. *Marine Chemistry*, *91*(1), 37–51. https://doi.org/10.1016/j.marchem.2004.04.003

Reeburgh, W. S. (1967). An improved interstitial water sampler. *Limnology and Oceanography*, *12*(1), 163–165. https://doi.org/10.4319/lo.1967.12.1.0163

Risgaard-Petersen, N., Nielsen, L. P., Rysgaard, S., Dalsgaard, T., & Meyer, R. L. (2003). Application of the isotope pairing technique in sediments where anammox and denitrification coexist. *Limnology and Oceanography: Methods*, *1*(1), 63–73. https://doi.org/10.4319/lom.2003.1.63

Rousseau, S., Lavoie, D., Jutras, M., & Chassé, J. (2025). Transit time of deep and intermediate waters in the Gulf of St. Lawrence. *Ocean Modelling*, *195*, 102526. https://doi.org/10.1016/j.ocemod.2025.102526

Saucier, F. J., Roy, F., Senneville, S., Smith, G., Lefaivre, D., Zakardjian, B., & Dumais, J.-F. (2009). Modélisation de la circulation dans l'estuaire et le golfe du Saint-Laurent en réponse aux variations du débit d'eau douce et des vents. *Revue des Sciences de l'Eau*, *22*(2), 159–176. https://doi.org/10.7202/037480ar

Smith, J. N., & Schafer, C. T. (1999). Sedimentation, bioturbation, and Hg uptake in the sediments of the estuary and Gulf of St. Lawrence. *Limnology & Oceanography*, *44*(1), 207–219. https://doi.org/10.4319/lo.1999.44.1.0207

Smriga, S., Ciccarese, D., & Babbin, A. R. (2021). Denitrifying bacteria respond to and shape microscale gradients within particulate matrices. *Communications Biology*, *4*(1), 1–9. https://doi.org/10.1038/s42003-021-02102-4

Stevens, S. W., Pawlowicz, R., Tanhua, T., Gerke, L., Nesbitt, W. A., Drozdowski, A., et al. (2024). Deep inflow transport and dispersion in the Gulf of St. Lawrence revealed by a tracer release experiment. *Communications Earth & Environment*, *5*(1), 338. https://doi.org/10.1038/s43247-024-01505-5

Stief, P. (2013). Stimulation of microbial nitrogen cycling in aquatic ecosystems by benthic macrofauna: Mechanisms and environmental implications. *Biogeosciences*, *10*(12), 7829–7846. https://doi.org/10.5194/bg-10-7829-2013

Stief, P., Kamp, A., Thamdrup, B., & Glud, R. N. (2016). Anaerobic nitrogen turnover by sinking diatom aggregates at varying ambient oxygen levels. *Frontiers in Microbiology*, *7*, 98. https://doi.org/10.3389/fmicb.2016.00098

Stief, P., Lundgaard, A. S. B., Morales-Ramírez, Á., Thamdrup, B., & Glud, R. N. (2017). Fixed-nitrogen loss associated with sinking zooplankton carcasses in a coastal oxygen minimum zone (Golfo Dulce, Costa Rica). *Frontiers in Marine Science*, *4*, 152. https://doi.org/10.3389/fmars.2017.00152

Stockdale, A., Davison, W., & Zhang, H. (2009). Micro-scale biogeochemical heterogeneity in sediments: A review of available technology and observed evidence. *Earth-Science Reviews*, *92*(1–2), 81–97. https://doi.org/10.1016/j.earscirev.2008.11.003

Tang, W., Tracey, J. C., Carroll, J., Wallace, E., Lee, J. A., Nathan, L., et al. (2022). Nitrous oxide production in the Chesapeake Bay. *Limnology and Oceanography*, *67*(9), 2101–2116. https://doi.org/10.1002/lno.12191

Thibodeau, B., Lehmann, M. F., Kowarzyk, J., Mucci, A., Gélinas, Y., Gilbert, D., et al. (2010). Benthic nutrient fluxes along the Laurentian Channel: Impacts on the N budget of the St. Lawrence marine system. *Estuarine, Coastal and Shelf Science*, *90*(4), 195–205. https://doi.org/10.1016/j.ecss.2010.08.015

Walter, S., Breitenbach, U., Bange, H. W., Nausch, G., & Wallace, D. W. R. (2006). Distribution of N_2O in the Baltic Sea during transition from anoxic to oxic conditions. *Biogeosciences*, *3*(4), 557–570. https://doi.org/10.5194/bg-3-557-2006

Wood, S. N. (2017). *Generalized additive models: An introduction with R* (2nd ed., p. 496). Chapman and Hall/CRC. https://doi.org/10.1201/9781315370279

Yin, G., Hou, L., Liu, M., Liu, Z., & Gardner, W. S. (2014). A novel membrane inlet mass spectrometer method to measure $^{15}NH_4^+$ for isotope-enrichment experiments in aquatic ecosystems. *Environmental Science \& Technology*, *48*(16), 9555–9562. https://doi.org/10.1021/es501261s

Zhou, J., Zheng, Y., Hou, L., An, Z., Chen, F., Liu, B., et al. (2023). Effects of acidification on nitrification and associated nitrous oxide emission in estuarine and coastal waters. *Nature Communications*, *14*(1), 1380. https://doi.org/10.1038/s41467-023-37104-9

References From the Supporting Information

Devine, L., Kennedy, M. K., St-Pierre, I., Lafleur, C., Ouellet, M., & Bond, S. (2014). *BioChem: The Fisheries and Oceans Canada database for biological and chemical data* (Canadian technical report of fisheries and aquatic sciences No. 3073) (p. 40). Science Branch, Department of Fisheries and Oceans Canada. Retrieved from http://cat.fsl-bsf.scitech.gc.ca/record=b4008162~S1